Multiscale Modelling of Moso Bamboo Oriented Strand Board

Patrick G. Dixon,[a] Sardar Malek,[a] Kate E. Semple,[b] Polo K. Zhang,[b] Gregory D. Smith,[b] and Lorna J. Gibson [a,*]

The modulus of elasticity (MOE) of three-layer moso bamboo (*Phyllostachys pubescens* Mazel) Oriented Strand Board (OSB) was modelled using a multiscale approach proposed for wood OSB. The modelling approach for wood OSB was adapted to bamboo OSB by accounting for the different structures of wood and bamboo tissue. The MOE of moso bamboo OSB was measured previously in bending; the strands in the surface layer had a preferred orientation and were either from the internode region of the culm or contained node tissue. The model for loading parallel to the preferred orientation of the surface strands gives a good description of the measured values of MOE for boards with internode surface strands (8.6 GPa modelled compared to 8.1 GPa previously measured), but overpredicts that for boards with surface strands containing nodes (8.8 GPa modelled compared to 6.7 previously measured). The model for loading perpendicular to the preferred orientation of the surface strands gives a good description of the MOE data if the core layer moduli are estimated using compliance averaging, for specimens with and without nodes (1.5 GPa modelled compared to 1.5 GPa previously measured).

Keywords: Bamboo; Oriented strand board; Multiscale modelling

Contact information: a: Department of Materials Science and Engineering, Massachusetts Institute of Technology, 77 Massachusetts Avenue, Cambridge, MA 02139 USA; b: Department of Wood Science, University of British Columbia , 2900-2424 Main Mall, Vancouver, BC V6T 1Z4 Canada;
** Corresponding author: ljgibson@mit.edu*

INTRODUCTION

The full potential of bamboo for structural applications has yet to be realized. The design and use of structural bamboo products (SBP) allows more efficient use of this renewable resource. Bamboo-bundle laminated veneer lumber, laminated bamboo lumber, and bamboo Oriented Strand Board (OSB) are examples of such possibilities (Mahdavi *et al.* 2011; Chen *et al.* 2014; Semple *et al.* 2015c). In particular, bamboo OSB can be used in paneling and sheathing applications, with reduced material waste compared to laminated boards. Bamboo OSB has great potential for industrial production, for example, in terms of consistent quality and efficiency of mass production (Semple *et al.* 2015c).

Bamboo has a considerably more heterogeneous structure than wood (Liese 1987; Sjöström 1993; Wegst 2011). The tissue is primarily composed of vascular bundles and parenchyma. The structure resembles a fiber-reinforced composite, with the vascular bundles (composed of fibers and conducting cells) and parenchyma acting analogous to fiber and matrix, respectively (Liese 1987; Amada *et al.* 1997). The volume fractions of vascular bundles and their associated fibers increase sharply radially, going from the inside to the outside of the culm wall (Liese 1987; Nogata and Takahashi 1995; Amada *et al.*

1997; Ghavami *et al.* 2003; Liu *et al.* 2014). This heterogeneity and the resulting density gradient are important to consider in manufacturing and modelling of structural bamboo products. For instance, the heterogeneous tissue of bamboo can lead to significant strand roughness, if not sliced cleanly (Semple *et al.* 2015a, b), which then could impact the bonding and performance of a bamboo product.

Wood OSB is widely used in sheathing and other applications (Hoadley 2000; Chapman 2006). Strands, which serve as the structural elements of the product, are cut from logs, then spray coated with resin. These coated strands are then formed into a mat, which undergoes a hot-pressing procedure, consolidating the mat into a board (Chapman 2006). Several interplaying phenomena occur in the mat during the pressing operation, including heat and mass transfer, water-steam phase change, resin curing, and consolidation, densification, and stress relaxation in the wood. These phenomena give rise to a density gradient generally characterized by high-density faces and a low-density core; the core typically has less densified material (Kamke and Casey 1988; Wolcott *et al.* 1994; Xu 1999; Wang and Winistorfer 2000; Winistorfer *et al.* 2000). The density gradients through the thickness of such composites are commonly referred to as vertical density profiles (VDPs). The VDP is critical to the mechanical performance of a board (Wang and Winistorfer 2000; Winistorfer *et al.* 2000; Wang *et al.* 2004; Painter *et al.* 2006a).

Early models for the mechanical properties of wood OSB assumed a uniform density profile (Shaler and Blankenhorn 1990; Xu and Suchsland 1998). Subsequently, laminate theory was used to model many layered boards with varying density in the different layers, resulting from the compaction of the strands during processing (Xu 1999). Painter and colleagues (2006a) constructed a model that predicts the VDP of OSB and then uses the framework of Xu and Suchsland (Xu and Suchsland 1998; Xu 1999) to predict the MOE of OSB (Painter *et al.* 2006b). A rigorous continuum micromechanics approach was taken by Stürzenbecher *et al.* (2008) to model veneer strand board, consisting of slender large area wood strands of uniform size and geometry. More recently, Malekmohammadi *et al.* (2015) developed a multiscale analytical modelling framework for predicting the MOE of OSB by accounting for the board's properties at three length scales: micro, meso, and macro. The latter, more comprehensive framework provides a multiscale approach to modelling OSB, permitting adjustments for different types of plant tissues, such as bamboo, other grasses, and palms. In this study, this multiscale approach was adapted to model the flexural modulus of bamboo oriented strand board; the model is described in more detail in the modelling section.

Using *Phyllostachys pubescens* Mazel, or moso bamboo, Lee *et al.* (1996) demonstrated that it is possible to manufacture bamboo OSB and that its properties could meet industrial requirements. The effects of strand orientation in the board layers, board density, and strand length on the properties of moso bamboo OSB have been reported previously (Sumardi *et al.* 2007; Sumardi and Suzuki 2013; Sumardi *et al.* 2015). Recently, the fabrication and properties of moso bamboo OSB (Semple *et al.* 2015c, d), as well as details regarding moso and *Guadua angustifolia* Kunth bamboo strand production and classification, have been documented (Semple *et al.* 2015a, b). Moso OSB is stronger than wood analogs, but similarly stiff (Lee *et al.* 1996; Semple *et al.* 2015c).

This study models the MOE of moso bamboo OSB, using the approach of Malekmohammadi *et al.* (2015) to relate the properties of bamboo tissue to those of strand-based bamboo products – specifically, the three-layer pure moso (core and surface moso furnish) OSB manufactured by Semple *et al*. (2015c). These boards had average densities (700 to 720 kg/m^3) and MOEs (6 to 9 GPa) (Semple *et al.* 2015c) along the parallel

direction slightly above the ranges reported for aspen OSB (450 to 710 kg/m^3 and 4 to 8 GPa) by Chen *et al.* (2010). Thus, they have potential for construction, and merit study. The model results are compared to previously measured values of MOE for the moso bamboo OSB boards (Semple *et al.* 2015c). This comparison is made to only assess initial validity of the model. For full model verification a larger statistically valid sample size is needed to capture the variability of bamboo OSB. The primary objective of this work is to present a model for bamboo OSB built on data. The presented model would enable the design of an extensive program in the future.

EXPERIMENTAL

Materials

The moso OSB boards modelled in this study were three-layer boards, with oriented strands in the faces and random strands in the cores, manufactured and experimentally characterized by Semple *et al*. (2015c). In addition to the strands, all three layers had intermediates and fines. Furnish classified as intermediates was treated as strands in the model. All of the furnish was moso bamboo, and the resin was phenol formaldehyde (PF). Two types of the boards were manufactured and modelled: one with surface strands containing no nodes, referred to as internode, and the other with surface strands containing nodes, referred to as node. Details regarding the manufacture and testing of these materials can be found in the work of Semple *et al.* (2015c, d).

Methods

VDP characterization

The distribution of density though the thickness of the boards was measured using an X-ray density profilometer (Model QDP-01X, Quintek Measurement Systems, Knoxville, TN) at intervals of 0.1 mm through the thickness of each specimen measuring 50 mm by 50 mm square. The VD profiler constructed an average profile from 10 specimens evenly distributed over the board and cut adjacent to the bending specimens, with four boards total, representing two internode boards and two node boards. Data for the density of the actual bending test specimens were not available for model development, and so the density of the adjacent VDP specimens was considered to be representative of the density of the rest of the board and test specimens.

Strand orientation distribution characterization

Three 150 mm by 150 mm sections of internode moso OSB were used to characterize the in-plane strand orientation distribution. To characterize the distribution throughout the board, layers were removed by milling. Images of the boards were captured at the top surface, mid-depth in the surface layer, the initial core surface, and mid-depth in the core layer (which was mid-depth of the entire board). A digital camera (Nikon J1 Model, Melville, NY) was used to capture images, which were then analyzed manually in Image J software (National Institutes of Health; https://imagej.nih.gov/ij/) to determine the strand orientation distribution.

Modelling

As shown schematically in Fig. 1, the board properties were calculated, considering three length scales: micro (the bamboo strand), meso (the strand and resin), and macro (a

thin sublayer with a distribution of strands and the entire board). Several parameters, such as compacted strand densities and thicknesses; strand, fines, resin, and void volume fractions; and resin coverage characteristics (resin thickness and resin area coverage) in the different layers of the board were needed in this approach. In a preprocessing step, these layer parameters were back-calculated from the board data such as the board resin content, fines content, density profile, *etc.* These parameters were then used in the following steps. In the micro-mechanical step, the compacted strand densities (calculated in the preprocessing step), and the inputs of a density-Young's modulus relationship and bamboo elastic constant ratios were used to calculate the strand properties in each layer. Subsequently, at the mesoscale these strand properties were used with the resin coverage characteristics (calculated in the preprocessing step) and estimated resin properties (which were inputs in this mesoscale step) to calculate the properties of the resin and bamboo composite strand. In the first macro-mechanical step, these composite resin bamboo strand properties were used with the strand orientation distribution, which was the external input of this step, to calculate layer properties. In the final step, the relevant layer properties were then integrated over the board thickness for effective rigidities, which are then used to calculate board MOEs on the parallel and perpendicular directions to the preferred strand orientation. The board and test geometry was the input of this final step. These steps of this model are discussed in more detail in this section.

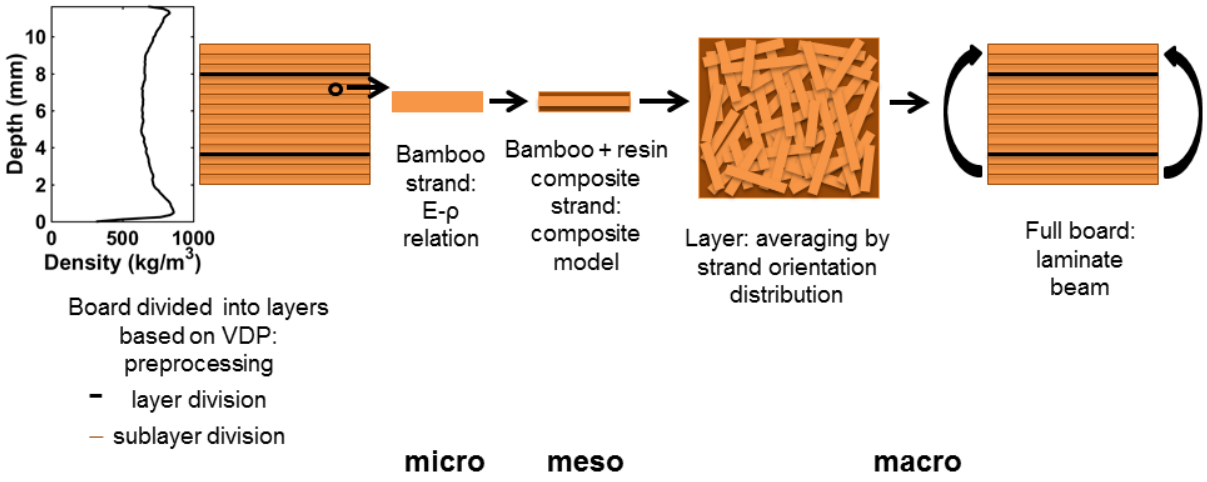

Fig. 1. Schematic of model framework

In the preprocessing step, boards were divided into roughly 100 sublayers based on experimental VDPs. The four measured summary VDPs, were employed for this purpose; two for boards with surface layers with internode strands and two for boards with surface layers with nodes in the strands.

The densities of the sublayers were determined from the VDPs and were combined with board data to calculate the inputs to the model, including resin, void, fines, and strand volume fractions; compacted strand thicknesses and densities; and resin coverage characteristics of each sublayer. Note that the board data is often documented by board manufacturers; thus many of the preprocessing input parameters' values are based on the work of Semple *et al.* (2015a, c, d). As previously noted, furnish classified as intermediates was treated as strands. These inputs are shown in Table 1.

Table 1. Preprocessing Inputs

$W_{strands}$[1]	W_{fines}[1]	W_{resin}[1,2]	W_{wax}[1,2]	ρ_{bamboo} (parent material)[1] (kg/m^3)	ρ_{resin}[3] (kg/m^3)	Strand length[4] (mm)	Strand width[4] (mm)	Strand thickness (uncompacted)[4] (mm)
81%	13%	6%	0%	745	1400	130	12.9	0.65

W refers to weight fraction. Furnish classified as intermediates is treated as fines. References: 1 (Semple *et al.* 2015c), 2 (Semple *et al.* 2015d), 3 (Malekmohammadi *et al.* 2015), 4 (Semple *et al.* 2015a)

The densities of the sublayers from the VDPs, PF resin weight fraction of 6% (Semple *et al.* 2015c, d), and assumed resin density of 1400 kg/m^3 (Malekmohammadi *et al.* 2015) are used to calculate resin volume fractions in each layer. Void volume fraction is then calculated similarly, with a parent material density of 745 kg/m^3 (Semple *et al.* 2015c) and assuming no densification in the core (minimum density layer in middle region of the board depth). The strand to fine weight ratio of the furnish is used with resin and void volume fractions to calculate their volume fractions and compacted densities (density of the fines and strands are equal in each layer) in each of the layers. Strand dimensions are taken simply by using moso strand dimension averages noted by Semple *et al.* (2015a), namely 0.65 mm for uncompacted thickness, 12.9 mm for width, and 130 mm for length. These dimensions (thickness corrected for compaction) and the calculated strand volume fraction are then used to estimate resin thickness, t_r. This thickness is then used with the resin volume fraction to calculate the resin area coverage. Further information on the preprocessing step can be found in Malekmohammadi *et al.* (2015).

In the micro-mechanical step, in contrast to Malekmohammadi *et al.* (2015), the longitudinal Young's moduli of the strands was estimated using the linear density-Young's modulus relationship given by Dixon and Gibson (2014) for internode material (see Fig. 2). The linear relationship used was empirical; a model for the longitudinal Young's modulus built from microstructural observations gives similar results (Dixon and Gibson 2014).

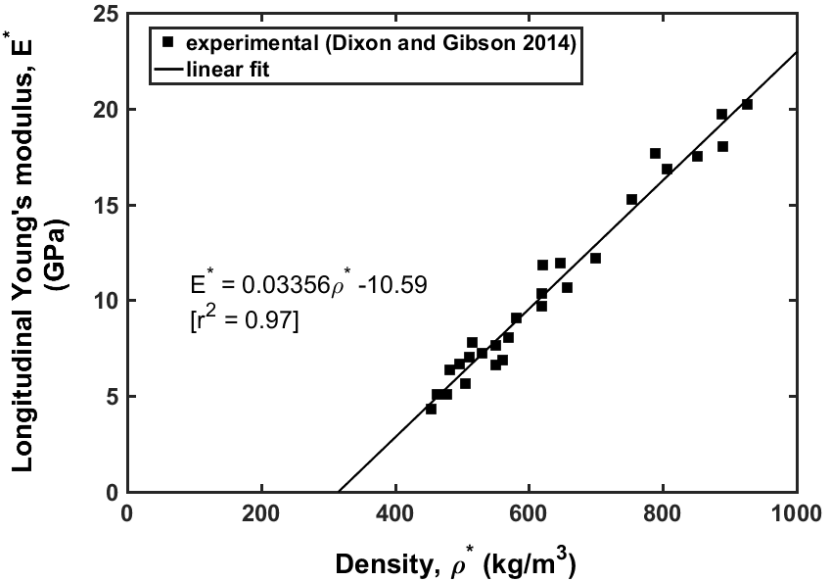

Fig. 2. Moso bamboo *E-ρ* relationship for specimens from the internodes

It should also be noted that this relationship, used to calculate longitudinal strand Young's moduli, was obtained from bending tests on small samples (n = 27), cut from different positions in a moso bamboo culm section (Dixon and Gibson 2014). The longitudinal MOE was approximated as the longitudinal Young's modulus, E^*; shearing effects were negligible because the span to depth ratio of the beams was greater than 20.

While the density-Young's modulus relationship that was used in the model is empirical, it has microstructural justification. As noted previously, the microstructure of bamboo is similar to a unidirectional fiber-reinforced composite. The density, ρ^* (kg/m^3), of such a structure is given by the rule of mixtures (treating all non-fiber tissue as parenchyma matrix, $V_f = 1 - V_m$),

$$\rho^* = \rho_f V_f + \rho_m V_m \quad (1)$$

where, ρ and V denote densities (kg/m^3) and volume fractions, respectively, and the subscripts f and m refer to the fibers (fibers) and matrix (parenchyma), respectively.

The longitudinal Young's modulus, E^* (GPa) follows the same rule of mixtures,

$$E^* = E_f V_f + E_m V_m \quad (2)$$

in which E refers to Young's modulus (GPa). Combining Eq. 1 and Eq. 2 results in a linear density-Young's modulus relationship,

$$E^* = \frac{E_f - E_m}{\rho_f - \rho_m}\rho^* + \frac{E_m \rho_f - E_f \rho_m}{\rho_f - \rho_m} \quad (3)$$

This is a departure from the approach of Malekmohammadi *et al*. (2015), accounting for the different microstructures of wood and bamboo, while retaining the analytical nature of the wood micro-mechanical relationship of Gibson and Ashby (1997) used in the framework of Malekmohammadi *et al.* (2015). This relationship, developed from internode material, is applied to the boards composed of surface strands both without and with nodes; the nodes are not accounted for at the microscale. Notably, other linear fits with different constants for bamboo developed in the future (be it for tissue of other species, harvested from a particular location, *etc.*) could be easily exchanged here in this framework.

The ratios of the Young's moduli along the tangential and radial directions and all the shear moduli to the longitudinal Young's modulus for moso bamboo are given by Bai (1996) in Table 2.

These ratios are used to calculate the radial and tangential Young's moduli and the shear moduli of the strands. These ratios are assumed constant at all densities. Likewise, the Poisson's ratios are taken as constants at all densities (Bai 1996).

Table 2. Elastic Constant Ratios (Bai 1996)

E_T/E_L	E_R/E_L	G_{LT}/E_L	G_{LR}/E_L	G_{RT}/E_L	ν_{LT}	ν_{LR}	ν_{RT}
0.053	0.069	0.085	0.079	0.028	0.341	0.390	0.308
E refers to Young's modulus, G to shear modulus, and ν to Poisson's ratio. L, T, and R refer to the longitudinal, tangential, and radial directions of the wood respectively.							

In the mesoscale step, analytical micromechanics equations, developed by Malekmohammadi *et al.* (2014) were then applied to calculate the properties of the unit cell, namely, a bamboo strand covered in resin. These equations, which can be found in Malekmohammadi *et al.* (2014), were developed from the application of iso-stress conditions followed by iso-strain conditions on a strand completely covered with resin. The resin's Young's modulus, E_r (GPa), was taken to be 7.60 GPa, the value taken by Malekmohammadi *et al.* (2015) to model experimental boards also made with PF resin manufactured by Chen *et al.* (2010); assuming isotropy and using a Poisson's ratio of 0.3, its shear modulus was taken to be 2.92 GPa. It is also noted the values of these elastic properties and the resin density of 1400 kg/m^3 are quite typical when the properties of phenol formaldehyde resins are viewed in CES Selector 2016, materials selection software by Granta Design (Cambridge, UK). The correction for partial strand coverage by the resin, given by Malekmohammadi *et al.* (2014), was then made. Poisson's ratios of the unit cell, developed with similar treatment, are more involved expressions, which can be found in Malekmohammadi *et al.* (2014). For simplicity, in this work the Poisson's ratios of the combined bamboo and resin strand were taken to be the same as those of the bamboo strand (Table 2).

In the macroscale step, the local (meaning local to the strand as opposed to global of the board) stiffness and compliance matrices, C_{ij} (GPa) and S_{ij} (GPa^{-1}), respectively, were transformed to those of the strand at an orientation angle ϕ (°), $C_{ij,\phi}$ and $S_{ij,\phi}$, and then weighted, based on the experimentally determined strand orientation distribution, to obtain the matrices for the sublayer, $\overline{C_{ij}}$ and $\overline{S_{ij}}$. Several researchers simply used the Hankinson formula (Shaler and Blankenhorn 1990; Xu and Suchsland 1998; Barnes 2000; Painter *et al.* 2006b), while matrix transformation is a more general approach that Malekmohammadi *et al.* (2015) employed.

The surface-core boundaries were determined from the core and surface full layer densities and total board densities noted by Semple *et al.* (2015c). Matrices were transformed at angles, ϕ, of -85° to 85° in 10° increments and weighted by frequency (count fraction), f_ϕ, in the surrounding 10° of the rotation angle. For the core sublayers, a uniform distribution was used rather than the experimentally obtained one; *i.e.*, a constant weight was used for all angles. This weighting assumes the count fraction (*i.e.*, the frequency) equals the volume fraction, and strand geometry, size, and size distribution are not considered in the averaging. This is a considerable, but practical, simplification.

Only stiffness averaging is used in the framework of Malekmohammadi *et al.* (2015). Similarly, previous OSB models took only an upper bound approach (Xu and Suchsland 1998; Painter *et al.* 2006b). However, in the current work the stiffness averaging is used for the relatively aligned faces for the parallel MOE model (for loading parallel to the preferred strand orientation), but the compliance averaging method is used for the faces for the perpendicular MOE model (for loading perpendicular to the preferred strand orientation). The logic is based on the faces' relatively high alignment with the parallel loading direction. For the randomly oriented core sublayers, there is no preferred strand orientation, and the effective elastic properties are expected to lie between those obtained from stiffness or compliance averaging. Therefore, both averaging methods are applied to the core. Expressions for the averaging methods are shown below. Equation 4 is the stiffness averaging equation, and Eq. 5 is the compliance averaging equation (Pastore and Gowayed 1994),

$$\overline{C_{ij}} = \sum f_{\phi} C_{ij,\phi} \quad (4)$$

$$\overline{S_{ij}} = \sum f_{\phi} S_{ij,\phi} \quad (5)$$

where f_{ϕ} is the fraction from the distributions, $C_{ij,\phi}$ and $S_{ij,\phi}$ are the transformed strand matrices, and $\overline{C_{ij}}$ and $\overline{S_{ij}}$ are the sublayer matrices. The local C_{ij} and S_{ij} are inverses of each other, and thus equivalent matrices, as are the transformed matrices, $C_{ij,\phi}$ and $S_{ij,\phi}$ at a given angle ϕ. The averaged sublayer matrices, $\overline{C_{ij}}$ and $\overline{S_{ij}}$, however, generally are not.

The extraction of the relevant Young's and shear moduli from the average matrix of each sublayer was then performed. For this purpose, the board was treated as a multilayer laminate beam, as in Malekmohammadi *et al.* (2015). Namely, sublayer properties were integrated over the board sections to determine the effective rigidities $(EI)_{eq}$ (GPa mm^4) and $(AG)_{eq}$ (GPa mm^2), given in Eqs. 6 and 7.

$$(EI)_{eq} = \int_{0-\bar{z}}^{t-\bar{z}} E_{sublayer} b z^2 dz \quad (6)$$

$$(AG)_{eq} = \int_{0-\bar{z}}^{t-\bar{z}} G_{sublayer} b dz \quad (7)$$

In Eqs. 6 and 7, $E_{sublayer}$ (GPa) and $G_{sublayer}$ (GPa) are the relevant moduli of the sublayers, b is the width (mm), t is the total board thickness (mm), and $\bar{z}$ is the location of the neutral axis (mm). Board compliances (δ/P) (mm/kN) are calculated for three-point bending, the loading configuration used in the tests by Semple *et al.* (2015a),

$$\frac{\delta}{P} = \frac{L^3}{48(EI)_{eq}} + \frac{L}{4(AG)_{eq}} \quad (8)$$

where L (mm) is the span of the beam (Allen 1969). The MOEs of the board in parallel and perpendicular directions were then determined using the compliance values estimated from the above equation.

RESULTS AND DISCUSSION

VDPs

The measured experimental summary VDPs are shown in Fig. 3. These four VDPs were used as inputs to the model. They all show the typical high density surfaces and lower density core common of oriented strand board (Xu 1999; Wang and Winistorfer 2000; Winistorfer *et al.* 2000).

Strand Orientation Distribution

Figure 4 shows images of the surface (a) and core (b) with the measurements made in Image J for the strand orientation overlaid. The edges of both boards are approximately 150 mm.

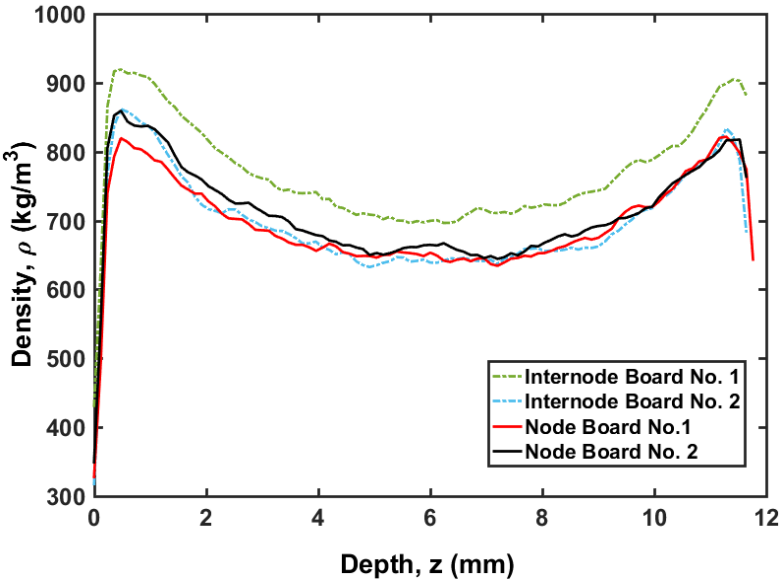

Fig. 3. Experimental summary VDPs

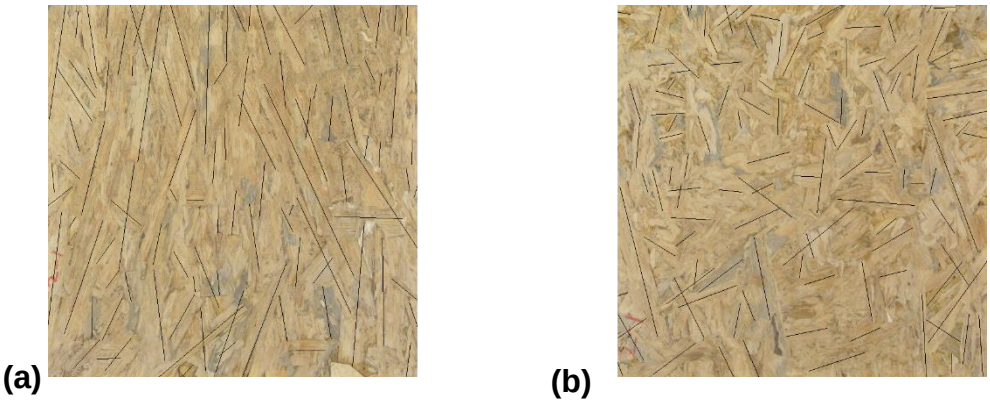

Fig. 4. Images of (a) the surface and (b) the core layers

Figure 5 shows the measured strand orientation distribution for the surface and the core layers.

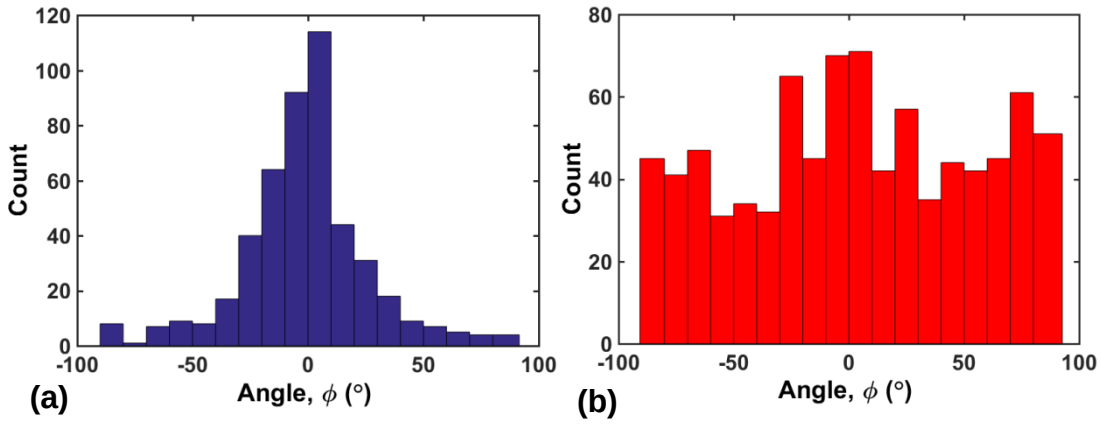

Fig. 5. Strand orientation distribution for (a) the surface and (b) the core layers

Figure 5(a) is the measured surface strand orientation distribution, used calculate average layer stiffness and compliance matrices for the surface sublayers. As previously mentioned, a uniform strand orientation distribution, opposed to the measured distribution, shown in Fig. 5(b), was used for calculation in the core sublayers.

MOE Predictions

The model estimates of the MOE of the boards, for the normal stresses in the boards parallel and perpendicular to the preferred orientation of the strands in the surface layers, are compared with the experimental values in Table 3, for boards with strand material from the internodes or with nodes. The densities of the individual board specimens used in the bending tests were not measured; however, density and VDPs were measured for a series of adjacent 50 mm by 50 mm specimens of boards used to test internal bond strength, giving densities representative of the modelled board materials and shown in Table 3.

There was relatively good agreement between the experimental values and the model predictions for the MOE of the OSB with internode strands, for loading parallel to the preferred strand orientation, especially for the case with the lower density VDP of internode board no. 2 as input, which is probably closer to the density of the tested boards. The agreement was less good for the OSB with surface strands containing nodes, for loading parallel to the preferred strand orientation; this was probably due to a reduction in the strand stiffness associated with the nodes and also interference of the more heterogeneous node tissue in bonding and board consolidation during pressing. For loading perpendicular to the preferred strand orientation, there was good agreement between the model and the experimental values for both the OSB with internode strands and strands with nodes, if compliance averaging is used to estimate the core properties in the model. It should be clearly noted that this comparison between the modelled and experimental board MOE is preliminary and qualitative in nature, the sample size is too small for statistical comparison. However, the similarities and differences between the results will be discussed further to illustrate aspects of the model and bamboo.

Table 3. Modulus of Elasticity: Comparison of Models and Measurements

Model	Internode 1		Internode 2		Node 1		Node 2	
	MOE ll	MOE L	MOE ll	MOE L	MOE ll	MOE L	MOE ll	MOE L
Stiffness Averaging Core (GPa)	9.6	2.7	8.5	2.4	8.8	1.9	9.2	1.9
Compliance Averaging Core (GPa)	8.6	1.7	7.6	1.5	8.4	1.4	8.7	1.5
Density (kg/m^3)	770		697		695		710	
Measurements	Internode				Node			
	MOE ll	MOE L			MOE ll	MOE L		
(GPa)	8.09 ± 0.54	1.58 ± 0.52			6.67 ± 0.49	1.40 ± 0.38		
Board Type Density (kg/m^3)	713.4				706.0			

Note: Experimental results from Semple *et al.* (Semple *et al.*, 2015c). ll – parallel to preferred strand orientation, L – perpendicular to preferred strand orientation

For boards made with internode strands and with strands with nodes, the model predictions are similar. The linear density-Young's modulus relationship of moso bamboo used in the model was obtained for internode material only (Dixon and Gibson 2014). The presence of nodes in strands may reduce their MOE, as postulated by Semple *et al*. (2015c). The effect of nodes on the bending properties of bamboo is not yet clearly understood; the literature is mixed on their effect (Lee *et al.* 1994; Hamdan *et al.* 2009; de Vos 2010; Shao *et al.* 2010; Semple *et al.* 2013). Hamdan *et al.* (2009) found that nodes generally decrease both the longitudinal MOE and MOR in *Gigantochloa scortechinii* bamboo specimens in bending, but in general, the decrease was statistically significant only for the MOE. Conversely, Lee *et al.* (1994) found that only the MOR is influenced by the presence of a node. Similarly, Semple *et al.* (2013) using small bar (5 mm thick by 19 mm wide) flexural tests found nodes significantly reduced MOR in raw dry moso bamboo tissue, but the effect was small and not significant for MOE. When the tissue was compressed to 50% thickness under controlled steam injection conditions, the difference in MOR between internode and node tissue was amplified, but there was still relatively little effect on MOE.

Even if strands with nodes did not have lower longitudinal MOE of the moso tissue itself, nodes are sites of roughness and unevenness in strands reducing adhesion and consolidation, and contributing to lower board properties. This might be expected to also reduce experimental MOE perpendicular to the direction of strand orientation, relative to the internode values. Little reduction for loading in the perpendicular direction is observed (Semple *et al.* 2015c). The high degree of surface strand alignment along the parallel direction minimized the interlocking of strands along the perpendicular direction resulting in much lower perpendicular MOE and MOR values for boards, likely masking the node-induced bonding and consolidation effects influencing the parallel flexural properties. It is also possible that MOE does become affected by node tissue if the test specimen is very thin, such as a strand, which was not accounted for by the model. As Semple *et al.* (2015c) note, the effect of nodes on the mechanical and bonding behavior of strands needs to be understood in future research, in order to best address the problem of lower board MOE as a result of nodes in a practical manner, *i.e*., without removing all nodes from the material used for furnish.

A more detailed view of the results gives additional insights. The different averaging methods in the core lead to a difference in the model MOE for loading parallel to the preferred orientation of the strands of 0.4 to 1 GPa, or an average difference of roughly 10%, for boards made from internode strands. For loading in the perpendicular direction, for boards with internode strands, the difference in averaging methods gives a difference similar to that for loading in the parallel direction in absolute value and thus much higher in relative terms. This result is unsurprising, given that in the perpendicular loading direction, the denser faces do not dominate the MOE as they do in the parallel direction; the core, even with its uniform (random) orientation distribution, contributes significantly to the board MOE. The model MOEs of the boards made from strands with nodes show less difference between compliance and stiffness averaging methods in the core for both loading directions. The smaller difference, here, is due to the thicker surfaces of the boards, which were obtained with the general values given for the total board, surface, and core layer densities by Semple and her co-workers (2015c).

The model results using compliance averaging method in the core predict the experimental results better, especially so for loading in the perpendicular direction. This would suggest compliance averaging is the appropriate method for estimating the elastic properties of the core. However, there are a number of aspects in the modelling, for which

an overprediction of MOE might be expected. Chief among these is the uncertainty in the bamboo strand elastic properties. Uncertainty in the longitudinal Young's modulus and the elastic constant ratios of the bamboo strands as a result of moso bamboo's natural variability could increase or decrease the predicted results relative to the experimental data. In addition, the moisture content of the bamboo specimens, for which the E-ρ relationship was obtained, was quite low (~4%) (Dixon and Gibson 2014; Dixon *et al.* 2015); the moisture content of the bamboo strands in the boards is uncertain, but likely higher given the conditioning at two weeks at 65% relative humidity at 20 °C (Semple *et al.* 2015c, d). Jiang *et al.* (2012) found a 1.56% average change in the longitudinal tensile Young's modulus (1.49% for bending) with 1% change in moisture content. Bai (1996) notes a moisture content of roughly 12% for their bamboo elastic properties tests, and the moisture content of bamboo strands in the board may well be lower, leading to possible under predictions of the other elastic properties. This suggests that the error stemming from moisture content differences, while uncertain, is likely small.

A more likely contributor to the possible overprediction by the model is that the E-ρ relationship was obtained for strands cut from a bamboo culm; these values do not account for any damage to the tissue resulting from processing. In the model, compaction increases the properties as would a natural density increase; this is the same as in the approach used for wood OSB (Malekmohammadi *et al.* 2015). However, for bamboo, this assumption is more problematic. In wood, differences in density stem from differences in the cell wall thickness relative to the cell wall lumen size (Gibson and Ashby 1997), whereas in natural bamboo, density differences are primarily due to differences in the fiber volume fraction (Dixon and Gibson 2014). Given bamboo's heterogeneous structure and the high density of many species' bamboo fibers (Parameswaran and Liese 1976; Liese 1987), the densification of bamboo would likely primarily densify the parenchyma, resulting in a larger fiber volume fraction, but one that is not as large as that of the natural material at this density. This differential densification would result in lower properties at a given density. The phenomenon of artificially increasing the fiber volume fraction through controlled densification but being unable to match the flexural properties of natural tissue from the outer culm wall that is naturally high density was observed by Semple *et al.* (2013) and discussed by Dixon *et al.* (2016). The interpretation and relating the present findings to wood OSB is further complicated by the observation by Semple *et al.* (2015c) that unlike wood, the bamboo tissue in the surfaces of the board, even adjacent to the platens, undergoes little densification during a typical hot press cycle for OSB.

These issues in the modelling, the small data set, and other issues (*e.g.*, intermediates' treatment as strands) limit the assessment of the core averaging methods. However, along the parallel direction the two different methods give very similar model results, and along the perpendicular direction the results are qualitatively similar. Further exploration of compliance averaging for both the properties of uniformly (randomly) aligned layers and the layer properties perpendicular to the aligned direction is warranted.

CONCLUSIONS

1. The MOE of moso bamboo OSB was predicted using a comprehensive multiscale approach for wood, with a simple microscale adjustment accounting for the different structures of wood and bamboo. Despite simplifications and limitations, the parallel MOE of the three-layer moso boards made with internode strands is predicted quite

well, showing an average relative error (average of both internode VDP models and averaging methods in the core) of roughly 10%.

2. The parallel MOE in the boards made with strands with nodes are overpredicted by the model, suggesting the presence of nodes in surface strands negatively impacts bamboo boards' MOE.
3. Model results for loading perpendicular to the preferred strand orientation qualitatively predicts the experimental results for both board types. However, along the perpendicular direction, the modelled results vary considerably based on the averaging method used in the core. Compliance averaging in the core sublayers gives results which give a good description of the measured values.

ACKNOWLEDGMENTS

This paper is based upon work supported by the National Science Foundation under OISE: 1258574. The views expressed in this paper are not endorsed by the National Science Foundation. Research at UBC on densification of bamboo was supported by the National Science and Engineering Research Council of Canada (NSERC). The authors are grateful to the Martin Family Society of Fellows for Sustainability for their support. The authors would also like to thank an anonymous reviewer on earlier work, who presented the linear E-ρ relationship of bamboo (Eq. 3).

REFERENCES CITED

Allen, H. G. (1969). *Analysis and Design of Structural Sandwich Panels*, Pergamon Press Ltd., Oxford, UK.

Amada, S., Ichikawa, Y., Munekata, T., Nagase, Y., and Shimizu, H. (1997). "Fiber texture and mechanical graded structure of bamboo," *Composites Part B: Engineering* 28(1-2), 13-20. DOI: 10.1016/S1359-8368(96)00020-0

Bai, X. (1996). *Experimental and Numerical Evaluations of Bamboo-based Composite Materials*, Ph.D Dissertation, Clemson University, Clemson, SC.

Barnes, D. (2000). "An integrated model of the effect of processing parameters on the strength properties of oriented strand wood products," *Forest Products Journal* 50(11-12), 33-42.

Chapman, K.M. (2006). "Wood-based panels: particleboard, fibreboards and oriented strand board" in: *Primary Wood Processing: Principles and Practice*, 2nd Ed., J.C.F. Walker (ed.), Springer, Dordrecht, Netherlands, pp. 427-475.

Chen, S., Du, C., and Wellwood, R. (2010). "Effect of panel density on major properties of oriented strandboard," *Wood and Fiber Science* 42(2), 177–184.

Chen, F., Jiang, Z., Deng, J., Wang, G., Zhang, D., Zhao, Q., Cai, L., and Shi, S. Q. (2014). "Evaluation of the uniformity of density and mechanical properties of bamboo-bundle laminated veneer lumber (BLVL)," *BioResources* 9(1), 554-565. DOI: 10.15376/biores.9.1.554-565

Dixon, P. G., Ahvenainen, P., Aijazi, A. N., Chen, S. H., Lin, S., Augusciak, P. K., Borrega, M., Svedström, K., and Gibson, L. J. (2015). "Comparison of the structure and flexural properties of moso, guadua, and tre gai bamboo," *Construction and*

Building Materials 90, 11-17. DOI: 10.1016/j.conbuildmat.2015.04.042

Dixon, P. G., and Gibson, L. J. (2014). "The structure and mechanics of moso bamboo material," *Journal of The Royal Society Interface* 11(99), 20140321. DOI: 10.1098/rsif.2014.0321

Dixon, P. G., Semple, K. E., Kutnar, A., Kamke, F. A., Smith, G. D., and Gibson, L. J. (2016). "Comparison of the flexural behavior of natural and thermo-hydro-mechanically densified moso bamboo," *European Journal of Wood and Wood Products* 74(5), 633-642. DOI: 10.1007/s00107-016-1047-9

Ghavami, K., Rodrigues, C. S., and Paciornik, S. (2003). "Bamboo: Functionally graded composite material," *Asian Journal of Civil Engineering (Building and Housing)* 4(1), 1-10. ISSN: 1563-0854

Gibson, L. J., and Ashby, M. F. (1997). *Cellular Solids: Structure and Properties*, 2nd Ed., Cambridge University Press, Cambridge, UK.

Hamdan, H., Anwar, U. M. K., Zaidon, A., and Tamizi, M. M. (2009). "Mechanical properties and failure behaviour of *Gigantochloa scortechinii*," *Journal of Tropical Forest Science* 21(4), 336-344. ISSN: 0128-1283

Hoadley, R. B. (2000). *Understanding Wood: A Craftsman's Guide to Wood Technology*, The Taunton Press, Inc., Newtown, CT.

Jiang, Z., Wang, H., Tian, G., Liu, X., and Yu, Y. (2012). "Sensitivity of several selected mechanical properties of moso bamboo to moisture content change under the fibre saturation point," *BioResources* 7(4), 5048-5058. DOI: 10.15376/biores.7.4.5048-5058

Kamke, F. A., and Casey, L. J. (1988). "Fundamentals of flakeboard manufacture: internal-mat conditions," *Forest Products Journal* 38(6), 38-44.

Lee, A. W. C., Bai, X., and Peralta, P. N. (1994). "Selected physical and mechanical properties of giant timber grown in South Carolina," *Forest Products Journal* 44(9), 40-46.

Lee, A. W. C., Bai, X., and Peralta, P. N. (1996). "Physical and mechanical properties of strandboard made from moso bamboo," *Forest Products Journal* 46(11-12), 84-88.

Liese, W. (1987). "Research on bamboo," *Wood Science and Technology* 21(3), 189-209. DOI: 10.1007/BF00351391

Liu, H., Jiang, Z., Zhang, X., Liu, X., and Sun, Z. (2014). "Effect of fiber on tensile properties of moso bamboo," *BioResources* 9(4), 6888-6898. DOI: 10.15376/biores.9.4.6888-6898

Mahdavi, M., Clouston, P. L., and Arwade, S. R. (2011). "Development of laminated bamboo lumber: Review of processing, performance, and economical considerations," *Journal of Materials in Civil Engineering* 23(7), 1036-1042. DOI: 10.1061/(ASCE)MT.1943-5533.0000253

Malekmohammadi, S., Tressou, B., Nadot-Martin, C., Ellyin, F., and Vaziri, R. (2014). "Analytical micromechanics equations for elastic and viscoelastic properties of strand-based composites," *Journal of Composite Materials* 48(15), 1857-1874. DOI: 10.1177/0021998313490977

Malekmohammadi, S., Zobeiry, N., Gereke, T., Tressou, B., and Vaziri, R. (2015). "A comprehensive multi-scale analytical modelling framework for predicting the mechanical properties of strand-based composites," *Wood Science and Technology* 49(1), 59-81. DOI: 10.1007/s00226-014-0682-8

Nogata, F., and Takahashi, H. (1995). "Intelligent functionally graded material: Bamboo," *Composites Engineering* 5(7), 743-751. DOI: 10.1016/0961-

9526(95)00037-N

Painter, G., Budman, H., and Pritzker, M. (2006a). "Prediction of oriented strand board properties from mat formation and compression operating conditions. Part 1. Horizontal density distribution and vertical density profile," *Wood Science and Technology* 40(2), 139-158. DOI: 10.1007/s00226-005-0044-7

Painter, G., Budman, H., and Pritzker, M. (2006b). "Prediction of oriented strand board properties from mat formation and compression operating conditions. Part 2: MOE prediction and process optimization," *Wood Science and Technology* 40(4), 291-307. DOI: 10.1007/s00226-005-0050-9

Parameswaran, N., and Liese, W. (1976). "On the fine structure of bamboo fibres," *Wood Science and Technology* 10(4), 231-246. DOI: 10.1007/BF00350830

Pastore, C. M., and Gowayed, Y. A. (1994). "A self-consistent fabric geometry model: Modification and application of a fabric geometry model to predict the elastic properties of textile composites," *Journal of Composites Technology and Research* 16(1), 32-36. DOI: 10.1520/CTR10392J

Semple, K. E., Kamke, F. A., Kutnar, A., and Smith, G. D. (2013). "Exploratory thermal-hydro-mechanical modification (THM) of moso bamboo (*Phyllostachys pubescens* Mazel)," in: *Characterisation of Modified Wood in Relation to Wood Bonding and Coating Performance*, Rogla, Slovenia, 220-227.

Semple, K. E., Zhang, P. K., and Smith, G. D. (2015a). "Stranding moso and guadua bamboo. Part I. Strand production and size classification," *BioResources* 10(3), 4048-4064. DOI: 10.15376/biores.10.3.4048-4064

Semple, K. E., Zhang, P. K., and Smith, G. D. (2015b). "Stranding moso and guadua bamboo. Part II. Strand surface roughness and classification," *BioResources* 10(3), 4599-4612. DOI: 10.15376/biores.10.3.4599-4612

Semple, K. E., Zhang, P. K., and Smith, G. D. (2015c). "Hybrid oriented strand boards made from moso bamboo (*Phyllostachys pubescens* Mazel) and Aspen (*Populus tremuloides* Michx.): species-separated three-layer boards," *European Journal of Wood and Wood Products* 73(4), 527-536. DOI: 10.1007/s00107-015-0914-0

Semple, K. E., Zhang, P. K., Smola, M., and Smith, G. D. (2015d). "Hybrid oriented strand boards made from moso bamboo (*Phyllostachys pubescens* Mazel) and aspen (*Populus tremuloides* Michx.): uniformly mixed single layer uni-directional boards," *European Journal of Wood and Wood Products* 73(4), 515-525. DOI: 10.1007/s00107-015-0913-1

Shaler, S. M., and Blankenhorn, P. R. (1990). "Composite model prediction of elastic moduli for flakeboard," *Wood and Fiber Science* 22(3), 246-261. ISSN: 0735-6161

Shao, Z. P., Zhou, L., Liu, Y. M., Wu, Z. M., and Arnaud, C. (2010). "Differences in structure and strength between internode and node sections of moso bamboo," *Journal of Tropical Forest Science* 22(2), 133-138.

Sjöström, E. (1993). *Wood Chemistry: Fundamentals and Applications*, 2nd Ed., Academic Press, San Diego, CA.

Stürzenbecher, R., Hofstetter, K., Bogensperger, T., Schickhofer, G., and Eberhardsteiner, J. (2008). "A continuum micromechanics approach to elasticity of strand-based engineered wood products: Model development and experimental validation," in: *Composites with Micro-and Nano-Structure*, V. Kompis (ed.), Springer, Netherlands, pp. 161-179.

Sumardi, I., Ono, K., and Suzuki, S. (2007). "Effect of board density and layer structure on the mechanical properties of bamboo oriented strandboard," *Journal of Wood*

Science 53(6), 510-515. DOI: 10.1007/s10086-007-0893-9

Sumardi, I., and Suzuki, S. (2013). "Parameters of strand alignment distribution analysis and bamboo strandboard properties," *BioResources* 8(3), 4459-4467. DOI: 10.15376/biores.8.3.4459-4467

Sumardi, I., Suzuki, S., and Rahmawati, N. (2015). "Effect of board type on some properties of bamboo strandboard," *Journal of Mathematical and Fundamental Sciences* 47(1), 51-59. DOI: 10.5614/j.math.fund.sci.2015.47.1.4

de Vos, V. (2010). *Bamboo for Exterior Joinery: A Research in Material Properties and Market Perspectives*, BSc Thesis, University of Applied Sciences, Van Hall Larenstein (Wageningen, UR), Netherlands.

Wang, S., Winistorfer, P. M., and Young, T. M. (2004). "Fundamentals of vertical density profile formation in wood composites. Part III. MDF density formation during hot-pressing," *Wood and Fiber Science* 36(1), 17-25.

Wang, S., and Winistorfer, P. M. (2000). "Fundamentals of vertical density profile formation in wood composites. Part II. Methodology of vertical density formation under dynamic conditions," *Wood and Fiber Science* 32(2), 220-238.

Wegst, U. G. K. (2011). "Bending efficiency through property gradients in bamboo, palm, and wood-based composites," *Journal of the Mechanical Behavior of Biomedical Materials*, 4(5), 744–755. DOI: 10.1016/j.jmbbm.2011.02.013

Winistorfer, P. M., Moschler, W. W., Wang, S., DePaula, E., and Bledsoe, B. L. (2000). "Fundamentals of vertical density profile formation in wood composites. Part I. *In situ* density measurement of the consolidation process," *Wood and Fiber Science* 32(2), 209-219.

Wolcott, M. P., Kamke, F. A., and Dillard, D. A. (1994). "Fundamental aspects of wood deformation pertaining to manufacture of wood-based composites," *Wood and Fiber Science* 26(4), 496-511.

Xu, W. (1999). "Influence of vertical density distribution on bending modulus of elasticity of wood composite panels: A theoretical consideration," *Wood and Fiber Science* 31(3), 277-282.

Xu, W., and Suchsland, O. (1998). "Modulus of elasticity of wood composite panels with a uniform vertical density profile: A model," *Wood and Fiber Science* 30(3), 293-300.

Article submitted: December 6, 2016; Peer review completed: February 2, 2017; Revised version received and accepted: February 27, 2017; Published: March 13, 2017.
DOI: 10.15376/biores.12.2.3166-3181